Full Paper

Propellants, Explosives, Pyrotechnics

DOI: 10.1002/prep.201800215

The High-Pressure Characterization of Melt-Castable Energetic Materials: 3,3′-Bis-Oxadiazole-5,5′-Bis-Methylene Dinitrate

Jonathan C. Bennion,[a] Iskander G. Batyrev,[a] and Jennifer A. Ciezak-Jenkins*[a]

Abstract: The high-pressure behavior of 3,3′-bis-oxadiazole-5,5′-bis-methylene dinitrate (BODN) was studied at room temperature to 25 GPa by Raman spectroscopy and powder X-ray diffraction. The Raman spectra, powder patterns, and calculated unit-cell volumes at selected pressures show qualitative agreement with first-principles density function theory calculations. Over this pressure range, no evidence of polymorphism was observed which suggests that this energetic material can be formulated without the concern of forming lower-density phases at elevated pressures. Vibrational measurements suggest a reversible deformation of the C–C linkage between the oxadiazole rings with increased pressure.

Keywords: Melt-Cast · Explosives · High-Pressure

1 Introduction

The development of novel insensitive high-energy-density materials (HEDM) has been at the forefront of energetic materials research over the past few decades. Although several promising compounds have been developed to date, formulation issues have hindered their deployment as a military explosives [1]. In recent years, focus has shifted from insensitive munitions development to include the synthesis of novel melt-castable explosives. Ideally, a melt-castable material will possess well-defined characteristics including a high loading density, a low melting point (in the range of 70.0 to 120.0 °C), and significant separation between the temperature of melting and the temperature of decomposition. Traditionally, melt-cast technology has been dominated by the prototypical energetic material 2,4,6-trinitrotoluene (TNT). Although the performance of TNT is lower than that of many HEDMs, its continued use as both a military and industrial explosive arises from favorable materials properties, low production cost, insensitivity to external stimuli, as well as a low melting point (81.0 °C) [2].

Recently, many novel energetic materials have been synthesized which show potential for melt-castable applications [3], including novel HEDMs derivatives of bis-oxadiazoles such as 3,3′-bis-oxadiazole-5,5′-bis-methylene dinitrate (BODN) [3d], see Figure 1. BODN was found to crystallize in the triclinic space group *P-1* with lattice parameters of $\mathbf{Z}=1$ and $\mathbf{a}=4.8405(4)$ Å, $\mathbf{b}=6.0293(4)$ Å, $\mathbf{c}=9.4356(7)$ Å, $\boldsymbol{\alpha}=80.399(6)^\circ$, $\boldsymbol{\beta}=77.125(7)^\circ$, $\boldsymbol{\gamma}=78.831(6)^\circ$, and $\mathbf{V}=261.16(4)$ Å^3 [3d]. The unit cell has various inter-/intramolecular interactions which include C–H···nitro hydrogen bonding and nitro···π interactions with the bis-oxadiazole ring systems. The molecules of BODN extend throughout the crystalline lattice in linear tapes with extend in the crystal lattice through the formation of linear tapes with strong C–H···N hydrogen bonds between adjacent molecules and these tapes form offset stacks through π–π interactions. Characterization of the energetic performance of BODN showed physical properties which exceed that of TNT; high crystallographic density (1.83 g/cm^3 at 295 K), moderate oxygen content (%OB = −33.3) and favorable

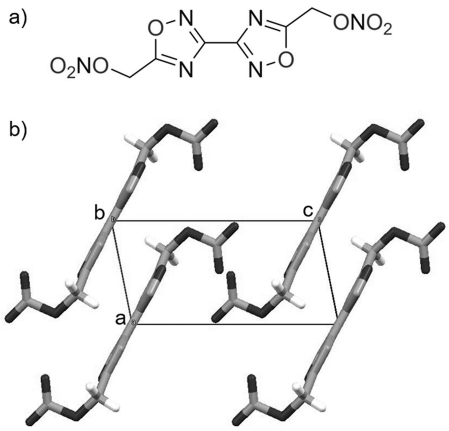

Figure 1. (a) Chemical structures of 3,3′-bis-oxadiazole-5,5′-bis-methylene dinitrate (BODN). (b) Crystal packing of the BODN unit cell viewed down the *b*-axis.

[a] *Dr. J. C. Bennion, Dr. I. G. Batyrev, Dr. J. A. Ciezak-Jenkins*
U.S. Army Research Laboratory
RDRL-WML-B, Aberdeen Proving Ground
Maryland 21005, United States
**e-mail: jennifer.a.ciezak-jenkins.civ@mail.mil*

 © 2019 Wiley-VCH Verlag GmbH & Co. KGaA, Weinheim

sensitivity properties. The predicted performance properties, both detonation velocity and detonation pressure, were determined to be 8180 m/s and 29.4 GPa, respectively. In addition to the promising energetic performance, BODN possesses the thermal properties necessary for melt-casting with a melting point of 84.5 °C and a 98.9 °C range before thermal decomposition. Sabatini *et al.* suggest that this powerful novel material can serve not only as an energetic plasticizing ingredient but also as a stand-alone melt-castable material to replace the lower-performing TNT [3d].

It is important to understand the thermomechanical and polymorphic behavior of energetic materials under high-pressure/temperature conditions, similar to those experienced during a detonation, before a novel material can be formulated on scale [4]. Conducting static high-pressure experiments is a crucial first step to understanding the behavior of a novel energetic in the run-up to detonation. Such measurements also yield valuable insight into how molecular deformation and inter-/intramolecular interactions are altered in response to extreme conditions and how the stability changes under high-pressure. The thermodynamic information obtained from such studies, such as the isothermal bulk modulus (B_0) and its pressure derivative (B'), is critical to aid hydrocode calculations in the accurate prediction of the performance properties of a novel energetic material. The performance and sensitivity of an energetic are highly dependent on a materials density and inter-/intramolecular interactions, both of which can vary considerably between different polymorphic phases. As such, it is essential to fully understand the polymorphic behavior of energetic materials under a variety of thermomechanical extremes and to understand the presence of any lower density polymorphs. High-pressure and/or high-temperature experiments have given access to additional metastable forms of both CL-20 and HMX [4a, 5].

The objective of the present study was to examine the isothermal structural stability and vibrational behavior of BODN when subjected to static high-pressure. The results from the Raman spectroscopy and powder X-ray diffraction studies provide strong evidence that the ambient pressure phase of BODN remains the dominate phase to near 25 GPa.

2 Experimental Section

BODN was obtained from the laboratory of Dr. J. Sabatini at ARL and used as synthesized. Isothermal high-pressure experiments were performed using piston-type symmetric diamond-anvil cells (DAC) with 300 μm culet type IIa diamonds. The sample was carefully ground into a fine powder before being loaded into a rhenium gasket with a sample well of ~120 μm diameter. A ruby sphere was placed in the sample well for the Raman spectroscopy experiments; in addition, gold flakes were added to sample well for the X-ray diffraction experiments. A helium pressure medium was loaded into the DACs using a high-pressure gas loading vessel previously described to generate quasi-hydrostatic conditions [6]. The pressure was determined within the DAC from the frequency shifts of the ruby R_1 and R_2 fluorescence lines before and after the Raman spectroscopy and X-ray diffraction experiments [7]. During the X-ray experiments, the in-situ pressure was determined using the 2Θ shift of gold [8].

Raman spectra were obtained on a custom-designed back-scattering Raman spectrometer with a 532 nm solid-state diode laser at a power of 10 mW. The scattered light from the sample was focused into a Princeton Instruments IsoPlane SCT320 monochromator with a grating of 1200 lines/mm and spectral resolution of 1.5 cm^{-1} before recording onto a PIXIS 400BR eXcelon CCD. Typical spectra were collected for 180 sec in the range of 100 to 4000 cm^{-1} to 25 GPa and analyzed using the LightField software package (Princeton Instruments). The Raman technique is detailed in previous publication [4b].

X-ray diffraction was performed at the Advanced Light Source (ALS) at Lawrence Berkeley National Laboratory on Beamline 12.2.2 to 25 GPa. For the present experiments, the X-ray beam was operated at 25 keV with a wavelength of 0.04973 nm for an average collection time per pattern of 90 seconds with a 3° rock of the DAC. To mitigate the X-ray damage to the samples during the collection, the beam was strongly attenuated and was rastered over the sample well. Structural parameters were derived from the diffraction patterns using Le Bail refinement within the Jade 9.0 software package [9]. Due to the large number of atoms per unit cell, along with the limited number of diffraction peaks refinement of the atomic positions with pressure was not attempted. The resulting pressure-volume data was analyzed with a third-order Birch-Murnaghan (BM) equation of state [10].

3 Computational Details

The crystalline structure of BODN with the triclinic space group *P-1* (CI-1), IT 2 corresponding to experimental crystallographic data at ambient condition (298 K, 0.0001 GPa) was relaxed using the plane wave code CASTEP [11] with the PBE functional [12]. Norm-conserving pseudo potentials [13] with a cut-off energy of 750 eV were used to obtain convergence criteria of total energy – better than 10^{-5} eV/at, eigenvalues – better that $0.45*10^{-6}$ eV and maximum force smaller than $3*10^{-3}$ eV/A. Van der Waals interactions were taken into account using dispersion corrections DF2 as developed by Grimme [14] and Tkatchenko-Scheffler [15] (TS). As the Tkatnchenko-Scheffler approximation gave slightly better agreement with experimental structural data (rms of deviation of lattice constants is 0.1025 Å for TS and 0.1808 Å for Grimme), this method was used for the calculation of vibrational spectra. For the calculation of dynamical matrix in the linear response theory [16], enhanced ac-

 © 2019 Wiley-VCH Verlag GmbH & Co. KGaA, Weinheim

curacy of convergence of eigenvalues of $0.45*10^{-10}$ eV was implemented. Density functional perturbation theory (DFPT) [11b] was used for calculations of Raman spectra using derivative of polarizability relative normal-mode coordinate derived in Porezag-Pederson [17]. For the DFPT solver, the all bands Gonze varational method [18] was used. Lorentzian broadening of 20 cm^{-1} and temperature smearing at 298 K were used for the calculation of Raman spectra.

4 Results and Discussion

4.1 Raman Spectroscopy

Selected Raman spectra of BODN subjected to isothermal compression to near 25 GPa are shown in Figure 2, with the Raman spectra truncated from 1300 to 1425 cm^{-1} and 1850 to 2850 cm^{-1} owing to strong diamond features. The spectra shown represent lattice phonons and internal skeletal vibrations of BODN, and can generally be assigned to the following vibrations: below 600 cm^{-1} (C–O–N wagging, CH_2 rocking, $CONO_2$ rocking), 600–1030 cm^{-1} (CH_2 rock and torsion, CC stretch/compression, oxadiazole ring in-/out-of-plane bending), 1130–1700 cm^{-1} (oxadiazole ring in-plane bending, oxadiazole ring stretching, NO_2 asymmetric stretching), 2850–3100 cm^{-1} (CH_2 stretch [symmetric/asymmetric]). The computational assignment of the strong Raman active modes of BODN at ambient conditions are presented in Table 1.

The ambient pressure Raman spectra match well with the previously published vibrational spectra (infrared spectroscopy) of BODN [3d]. The majority of the peaks in the Raman spectra of BODN maintained strong intensity throughout the experiment, with peak broadening occurring above 11 GPa. The peak broadening is consistent with intensity loss also observed in the X-ray diffraction experiments and can be weakly attributed to degradation of the hydrostatic performance of the He pressure media. Changes occur in the line shapes of several features near 770 cm^{-1} above 11 GPa, which are associated with the stretching of the C–C linkage between the two oxadiazole rings. Splitting of this feature likely occurs as a result of the compression along the *a*-axis in the crystal lattice of BODN, which results

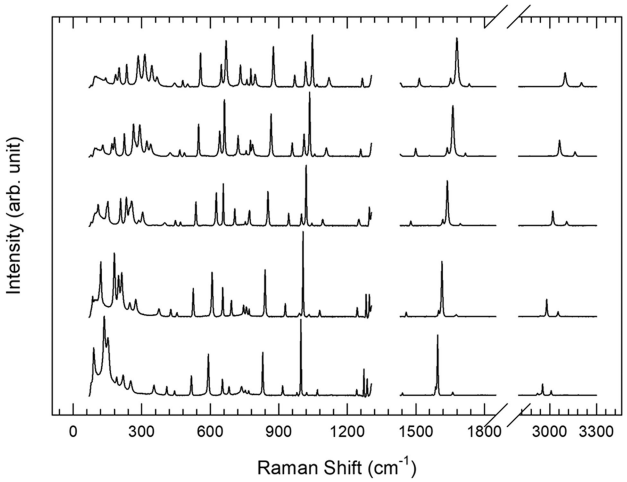

Figure 2. Representative Raman spectra of BODN. Spectra are offset for clarity. Note the peaks combining and subsequently splitting near 770 cm^{-1} above 11 GPa, which corresponds to the stretching of the C–C linkage between the two oxadiazole rings. The spectral regions from 1250 to 1475 cm^{-1} and 1900 to 2700 cm^{-1} is omitted due to the strong first-order and second-order scattering of the diamond anvils, respectively.

Table 1. BODN Raman Frequency Shifts (in cm^{-1}) at Ambient Pressure and Assignments.

Wavenumber [cm^{-1}]	Description of the crystalline mode
43	Rocking of whole molecule
63	Collective rotation of NO_2 and CH_2
76	Collective rocking of whole molecule
122	Rocking of oxadiazoles
131	Rocking of the whole molecule
139	Twisting of N–Os
182	Out of phase rotations of planes of oxadiazoles
208	Rocking C–Hs
244	Rocking C–Hs
322	Rocking C–Hs
398	Rocking C–Hs
434	Out of phase rotation of oxadiazoles
494	Out of phase rotation of oxadiazoles
541	Rocking C–Hs
640	Rocking C–Hs
657	Scissoring of N–Hs
719	Stretching of C–C bonds between oxadiazole rings
758	Stretching of C–C bonds between oxadiazole rings
901	Compression of N–O bond in oxadiazole
949	Rocking of C–Hs
980	Combined rocking of one of the C–Hs and stretching of oxadiazole by simultaneous outward movement of N and O atoms in oxadiazole
1003	Combined rocking of C–Hs and stretching of N–C bonds in oxadiazoles
1052	Scissoring of CH_2 and minor compression/stretching of C–O bonds and C–C affecting NO_2 group and oxadiazole
1209	C–H twisting of one of the C–Hs
1217	C–H twisting
1255	C–H twisting
1321	C–H wagging
1383	C–H scissoring
1406	C–H scissoring
1527	C–C bond rocking
1542	C–C bond compression/expansion between oxadiazoles
1578	N–O stretch of nitro group
2961	C–H symmetrical stretch of the Hs
3032	C–H asymmetrical stretch of the Hs

 © 2019 Wiley-VCH Verlag GmbH & Co. KGaA, Weinheim

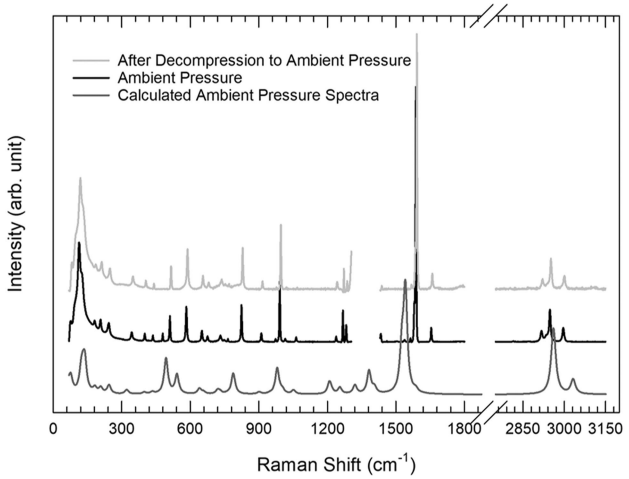

Figure 3. Comparison of Raman spectra of BODN at ambient pressure (black), after decompression (light gray) to ambient pressure, and the calculated Raman spectrum at ambient conditions (dark gray). Note the spectra of the decompressed BODN matches well with that of the as synthesized material. Although there is good qualitative agreement, the frequencies for some modes are quite different, especially around 1542 cm^{-1} region which is associated with the C–C bond compression/expansion between oxadiazoles. The spectral region from 1250 to 1475 cm^{-1} is omitted due to the strong first-order scattering of the diamond anvils.

in the C–C linkage between the oxadiazole rings deforming, *vide infra*. The shifting of peaks to higher wavenumbers as seen in the Raman spectra of BODN is consistent with deformation of the crystal lattice due to increased pressure; the presence of new features in the spectra would indicate the existence of polymorphism. Upon decompression, the sample could be quenched to the starting structure, as evidenced by the ambient pressure Raman spectra, with only slight modification of the peak intensity and bandwidth (Figure 3). The Raman spectra show good qualitative agreement with first-principles density function theory calculations (Figure 3).

Pressure-induced changes of the Raman frequencies of BODN is plotted as a function of pressure in Figure 4. Modes that have less than four pressure points have been omitted and the pressure dependence of the Raman shifts were fit with a second-order polynomial. As nearly all vibrational modes showed nearly linear slopes with increasing pressure, it can be suggested that no phase transitions occur in the material over the studied pressure range. This finding is in agreement with the trends noted in the X-ray diffraction experiments, as discussed below. The average peak shift value is 3.1 $cm^{-1}GPa^{-1}$, with a range between 0.8 and 8.3 cm^{-1} 1 GPa^{-1}; a value within the typical range for soft organic materials [4b]. The largest frequency shift (8.3 cm^{-1} 1 GPa^{-1}) in BODN occurs for the asymmetric stretch of the CH_2 hydrogens, and may indicate significant changes to the position of that CH_2 linkage with increased pressure.

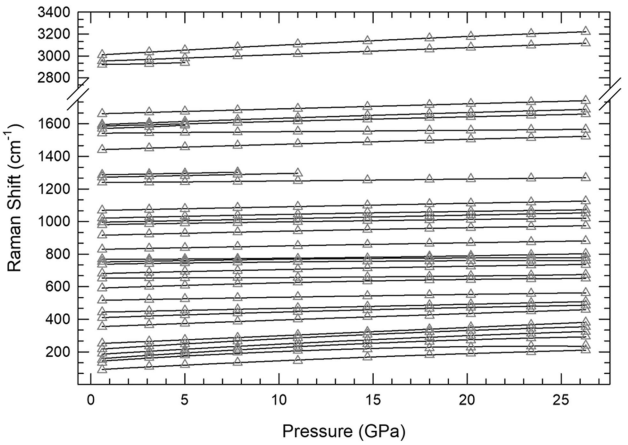

Figure 4. Pressure dependence of the peaks in the Raman spectrum of BODN. Frequency shifts have been fit to a second-order polynomial to help guide the eye.

4.2 Powder X-ray Diffraction

Analysis of the X-ray diffraction patterns of BODN at ambient conditions revealed triclinic *P-1* crystallographic structure, which is consistent with the structure previously identified. At ambient pressure the lattice parameters of BODN were found to be $\mathbf{a} = 4.8219(29)$ Å, $\mathbf{b} = 6.0199(30)$ Å, $\mathbf{c} = 9.4155(32)$ Å, $\boldsymbol{\alpha} = 78.973(35)^\circ$, $\boldsymbol{\beta} = 76.173(24)^\circ$, and $\boldsymbol{\gamma} = 77.364(21)^\circ$, which is in reasonable agreement with the previously published lattice parameters [3d]. Figure 5a shows the BODN PXRD features to near 25 GPa smoothly shift, which indicates that the *P-1* structure is maintained. The diffraction features in BODN maintained strong intensity throughout the experiment with minimal peak broadening occurring above 11 GPa. This trend is consistent with a gradual stress-induced amorphization, and loss of intensity can be correlated to thinning of the sample [19]. Shifting of the peaks with pressure is consistent with deformation of the crystal lattice at elevated pressure, with the peak arising from the (101) plane shifting most significantly. PXRD data is in full agreement with the results from the Raman spectroscopic experiments, with no evidence of a phase change observed over the pressure ranges of this study. The calculated powder patterns show good agreement with the experimental patterns (Figure 6) to 20 GPa. Upon decompression, BODN was found to have a diffraction pattern consistent with the observed pattern at ambient conditions, indicating complete recovery of the material (Figure 5b).

The pressure-volume isotherm at 298 K for BODN is shown in Figure 7a. Fitting of the experimental P–V data of BODN to a third-order Birch-Murnaghan equation of state [10] allows for the determination of the isothermal bulk modulus (B_0) and its pressure derivative (B') to 20 GPa. From this analysis, bulk modulus of $B_0 = 39.6 \pm 2.5$ GPa and pressure derivative of $B' = 8.7 \pm 1.4$ for BODN were derived. In-

 © 2019 Wiley-VCH Verlag GmbH & Co. KGaA, Weinheim

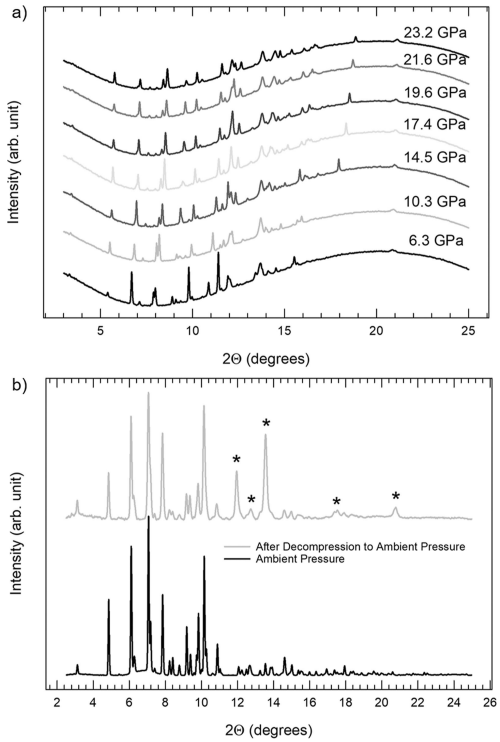

Figure 5. Selected X-ray diffraction patterns of (a) BODN collected as a function of pressure. The patterns are offset for clarity. Comparison of X-ray diffraction patterns of (b) BODN at ambient pressure (black) and after decompression (light gray) to ambient pressure. Peaks that appear in the patterns due to the rhenium gasket are marked with a black asterisk and spectra are background corrected for clarity.

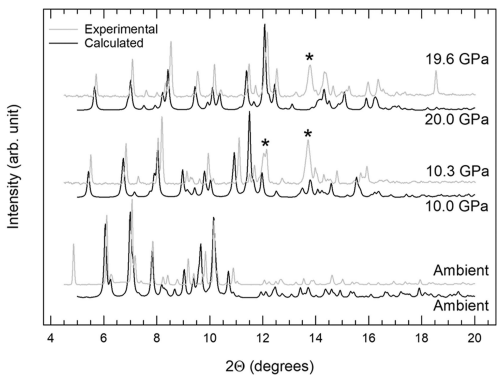

Figure 6. Comparison of experimental powder patterns (light gray) of BODN at ambient, 10.3 and 19.6 GPa pressures vs the calculated powder patterns (black) at ambient, 10.0 and 20 GPa pressures. Computed XRD patterns are calculated at the experimental wavelength of 0.4973 Å. Note that the calculated powder patterns of BODN match well with that of the experimental patterns, with the calculated patterns shifted to smaller 2Θ values at the respective pressures. Peaks that appear in the patterns due to the rhenium gasket are marked with a black asterisk (*).

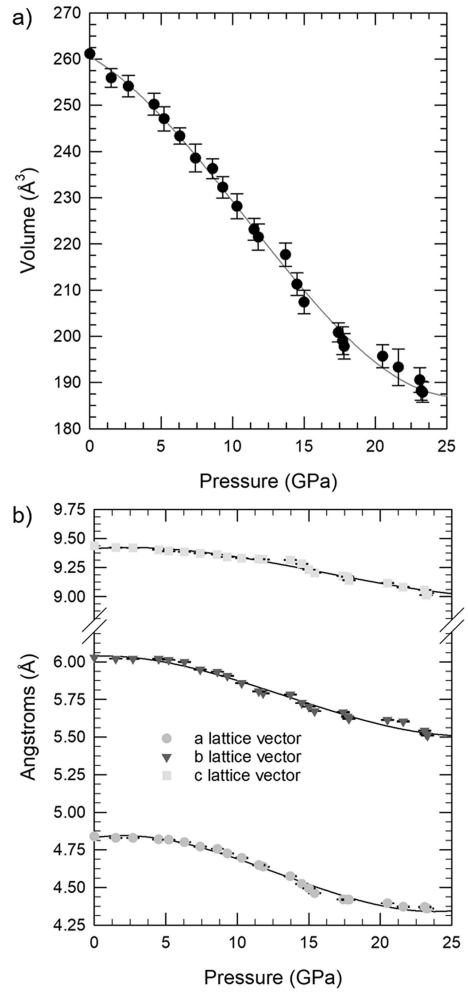

Figure 7. (a) Pressure-volume relationship of BODN upon compression based on unit-cell refinements using X-ray diffraction data. The compression data were fit to a third-order Birch-Murnaghan equation of state (solid line). (b) Pressure dependence of the lattice vectors of BODN upon compression. Points have been fit to a third-order polynomial to help guide the eye.

creasing the pressure from ambient conditions to 25 GPa in BODN resulted in total volume compression of 28.4 %.

Pressure-induced changes of the lattice parameters of BODN are represented in Figure 7b. All vectors show a smoothly varying monotonic decrease as a function of pressure, with the *a*-axis being the most compressible axis. This axis corresponds to the slipping plane of the slipped stack and likely results in an alteration of the $\pi-\pi$ interactions between adjacent molecules. The least compressible axis in BODN is the *c*-axis, and corresponds the compression of the stacks of the molecules of BODN.

© 2019 Wiley-VCH Verlag GmbH & Co. KGaA, Weinheim

5 Conclusions

The high-pressure behavior of 3,3′-bis-oxadiazole-5,5′-bis-methylene dinitrate (BODN) was examined with X-ray diffraction and Raman spectroscopy to pressures near 25 GPa. This study showed that the ambient pressure triclinic crystallographic structure of BODN remained stable under hydrostatic compression. The lack of polymorphism in this novel bis-oxadiazole energetic to 25 GPa suggests that this material can easily be formulated or melt-cast without the concern of forming lower density phases. This will not only aid in the speed of manufacturing, but with less steps in the manufacturing process needed to control the phase of the material the cost will also be reduced. Additionally, the important thermodynamic information obtained from this study is essential to the accuracy of theoretical predictions of the detonation properties of a novel energetic. These results are important for understanding the behavior of bis-oxadiazole energetic materials at high-pressure.

Acknowledgements

Dr. J. Sabatini is thanked for providing the BODN. During this project, coauthor J.C.B. was supported in full by an appointment to the Postdoctoral Research Program at the US Army Research Laboratory administered by the Oak Ridge Associated Universities. Portions of this work were performed at the Advanced Light Source, which is supported by the Director, Office of Science, Office of Basic Energy Sciences, of the U.S. Department of Energy under Contract No. DE-AC02-05CH11231.

References

[1] T. M. Klapötke, *Chemistry of High-Energy Materials*, 3 ed., Walter de Gruyter, Berlin/Boston, **2015**.

[2] R. Meyer, J. Köhler, A. Homburg, *Explosives*, Wiley-VCH, Weinheim, **2007**, pp. 307-360.

[3] a) J. C. Bennion, Z. R. Siddiqi, A. J. Matzger, A melt castable energetic cocrystal, *Chem. Commun.* **2017**, *53*, 6065–6068; b) L. A. Wingard, P. E. Guzmán, E. C. Johnson, J. J. Sabatini, G. W. Drake, E. F. C. Byrd, Synthesis of bis-Isoxazole-bis-Methylene Dinitrate: A Potential Nitrate Plasticizer and Melt-Castable Energetic Material, *ChemPlusChem* **2017**, *82*, 195–198; c) L. A. Wingard, E. C. Johnson, P. E. Guzmán, J. J. Sabatini, G. W. Drake, E. F. C. Byrd, R. C. Sausa, Synthesis of Biisoxazoletetrakis(methyl nitrate): A Potential Nitrate Plasticizer and Highly Explosive Material, *Eur. J. Org. Chem.* **2017**, *2017*, 1765–1768; d) E. C. Johnson, J. J. Sabatini, D. E. Chavez, R. C. Sausa, E. F. C. Byrd, L. A. Wingard, P. E. Guzmàn, Bis(1,2,4-oxadiazole)bis(methylene) Dinitrate: A High-Energy Melt-Castable Explosive and Energetic Propellant Plasticizing Ingredient, *Org. Process Res. Dev.* **2018**, *22*, 736–740.

[4] a) D. I. A. Millar, W. G. Marshall, I. D. H. Oswald, C. R. Pulham, High-pressure structural studies of energetic materials, *Crystallogr. Rev.* **2010**, *16*, 115–132; b) J. A. Ciezak, The High-Pressure Characterization of Energetic Materials: 1-Methyl-5-Nitramino-1H-Tetrazole, *Propellants Explos. Pyrotech.* **2010**, *35*, 373–378; c) J. A. Ciezak-Jenkins, G. M. Borstad, I. G. Batyrev, Characterization of the Isothermal Compression Behavior of LLM-172, *J. Phys. Chem. A* **2017**, *121*, 4263–4271.

[5] a) J. Bernstein, *Polymorphism in Molecular Crystals*, Oxford University Press Inc., New York, **2008**; b) J. A. Ciezak, T. A. Jenkins, Z. Liu, Evidence for a High-Pressure Phase Transition of ε-2,4,6,8,10,12-Hexanitrohexaazaisowurtzitane (CL-20) Using Vibrational Spectroscopy, *Propell. Explos. Pyrotech.* **2007**, *32*, 472–477.

[6] R. L. Mills, D. H. Liebenberg, J. C. Bronson, L. C. Schmidt, Procedure for loading diamond cells with high-pressure gas, *Rev. Sci. Instrum.* **1980**, *51*, 891–895.

[7] K. Syassen, Ruby under pressure, *High Pressure Res.* **2008**, *28*, 75–126.

[8] B. K. Godwal, A. Ng, R. Jeanloz, Gold under high pressure, *High Pressure Res.* **1992**, *10*, 687–693.

[9] *Jade 9.0 ed*, Materials Data, Inc, Livermore, CA, USA, **1995–2014**.

[10] F. Birch, Finite Elastic Strain of Cubic Crystals, *Phys. Rev.* **1947**, *71*, 809–824.

[11] a) M. D. Segall, J. D. L. Philip, M. J. Probert, C. J. Pickard, P. J. Hasnip, S. J. Clark, M. C. Payne, First-principles simulation: ideas, illustrations and the CASTEP code, *J. Phys.: Condens. Matter* **2002**, *14*, 2717; b) K. Refson, P. R. Tulip, S. J. Clark, Variational density-functional perturbation theory for dielectrics and lattice dynamics, *Phys. Rev. B* **2006**, *73*, 155114.

[12] J. P. Perdew, K. Burke, M. Ernzerhof, Generalized Gradient Approximation Made Simple, *Phys. Rev. Lett.* **1996**, *77*, 3865–3868.

[13] D. R. Hamann, M. Schlüter, C. Chiang, Norm-Conserving Pseudopotentials, *Phys. Rev. Lett.* **1979**, *43*, 1494–1497.

[14] S. Grimme, Semiempirical GGA-type density functional constructed with a long-range dispersion correction, *J. Comput. Chem.* **2006**, *27*, 1787–1799.

[15] A. Tkatchenko, M. Scheffler, Accurate Molecular Van Der Waals Interactions from Ground-State Electron Density and Free-Atom Reference Data, *Phys. Rev. Lett.* **2009**, *102*, 073005.

[16] S. Baroni, P. Giannozzi, A. Testa, Green's-function approach to linear response in solids, *Phys. Rev. Lett.* **1987**, *58*, 1861–1864.

[17] D. Porezag, M. R. Pederson, Infrared intensities and Raman-scattering activities within density-functional theory, *Phys. Rev. B* **1996**, *54*, 7830–7836.

[18] X. Gonze, Adiabatic density-functional perturbation theory, *Phys. Rev. A* **1995**, *52*, 1096–1114.

[19] H. Giefers, M. Pravica, Radiation-Induced Decomposition of PETN and TATB under Extreme Conditions, *J. Phys. Chem. A* **2008**, *112*, 3352–3359.

Manuscript received: July 2, 2018
Revised manuscript received: August 21, 2018
Version of record online: October 22, 2018

 © 2019 Wiley-VCH Verlag GmbH & Co. KGaA, Weinheim